"Characterization in a Wide Frequency Range (40 MHz - 67 GHz) of a KTa0.65Nb0.35O3 Thin Film for Tunable Applications"

Grégory Houzet, Thierry Lacrevaz, Cédric Bermond, Bernard Flechet, Arnaud Le Febvrier, Stéphanie Deputier, Maryline Guilloux-Viry, Patrick Queffelec

Characterization in a wide frequency range (40 MHz - 67 GHz) of a $KTa_{0.65}Nb_{0.35}O_3$ thin film for tunable applications

Grégory Houzet[a)], Thierry Lacrevaz, Cédric Bermond and Bernard Fléchet

IMEP-LAHC, UMR CNRS 5130, Université de Savoie, 73376 Le Bourget du Lac cedex, France.

Arnaud Le Febvrier, Stéphanie Députier, and Maryline Guilloux-Viry[b)]

ISCR, UMR CNRS 6226, Université de Rennes 1, 35042 Rennes cedex, France.

Patrick Queffelec[c)]

Lab-STICC, UMR CNRS 6285, Université de Bretagne Occidentale, 29238 Brest cedex 3, France.

a) gregory.houzet@univ-savoie.fr (Phone :+33479758658)

b) maryline.guilloux-viry@univ-rennes1.fr (Phone :+33223235655)

c) patrick.queffelec@univ-brest.fr (Phone :+33298016291)

Abstact

A (100) oriented $KTa_{0.65}Nb_{0.35}O_3$ 400 nm-thin film has been deposited by Pulsed Laser Deposition on MgO substrate. Microwave measurements, performed on InterDigitated Capacitors, show a paraelectric phase at room temperature with a tunability for the devices of 64% under an electric field of 400 kV/cm. Then, using a specific de-embedding method, the complex permittivity of the KTN thin film has been extracted from 40 MHz up to 67 GHz on coplanar waveguides. As promising applications are pointed out at 60 GHz, such as indoor communications, material characterizations are expected in this spectrum.

Keywords : Ferroelectric thin films, Microwave measurement, Parameter extraction, Tunable circuits and devices.

Shortened version of the title : Characterization up to 67 GHz of a KTN thin film.

1. INTRODUCTION

Ferroelectric oxides thin films are being explored in order to achieve high performance integrated systems. Indeed the richness of their properties open the way to a large variety of applications like Micro Electro Mechanical Systems, nonvolatile Ferroelectric Random Access Memories [1, 2], electrooptic waveguides [3], modulators or electrically tunable high frequency devices for telecommunication [4, 5]. For tunable microwave devices, a high tunability of the dielectric response is required under a moderate bias voltage, which is associated to a large change of the dielectric permittivity under an applied electric field. High performance devices require also low dielectric losses.

Furthermore, the ferroelectric thin film technology could be very attractive for millimeter wavelength applications, such as indoor communications (at 60 GHz), provided that material losses are controlled. Towards such future developments, it becomes of prime importance to characterize their dielectric properties in the aforementioned frequency bands. To compare with different technological solutions, we first focus on a commercial varactor diode solution [6]. In this reference, under a bias voltage of 10 V, a tunability of 26% is achieved at 2.3 GHz with a good quality factor of the structure. However, this solution is suitable at only low frequencies. Investigations are also performed on liquid crystals (LC) [7]. In this cited work, a tunability of 2% is obtained by changing the orientation of LC molecules by 90° at the frequency of 12 GHz. In this case, as birefringence of LC decreases at microwave frequencies, this solution could be suitable for operating frequencies in the infrared spectral region (for instance, a birefringence value as large as 0.21 is obtained in THz frequencies [8]). So, it exists a window of opportunity for ferroelectric thin film technology at microwave frequencies.

Among the possible oxide candidates, besides the $Ba_xSr_{1-x}TiO_3$ (or BST) which is the most extensively studied [9-12], $KTa_{1-x}Nb_xO_3$ (KTN) shows interesting properties: it presents high tunability in bulk [13] and thin films [14, 15]; its Curie temperature (T_C) can be tuned by adjusting the composition in the solid solution extending from $KTaO_3$ to $KNbO_3$ [16, 17] ; it can be expected to be deposited at lower temperature (of about 100°C) than titanates like BST for instance [18, 19]. Previous studies at microwave frequencies, have demonstrated promising dielectric features both for the $KTa_{0.65}Nb_{0.35}O_3$ [20] and $KTa_{0.50}Nb_{0.50}O_3$ [21] compositions, whose Curie temperature is expected to be slightly lower, or higher, than the room one, respectively. As device performances are directly linked with the dielectric properties of the film, it is of prime importance to have the knowledge of its complex permittivity in a wide frequency range. We report here a wide frequency range characterization of a $KTa_{0.65}Nb_{0.35}O_3$ (KTN) thin film grown on (100) MgO.

2. DEPOSITION AND PHYSICAL CHARACTERIZATION OF KTN THIN FILM

A 400 nm-thick KTN film has been deposited by pulsed laser deposition onto a 10 x 10 x 0.5 mm^3 (100) MgO substrate using a KrF excimer laser (λ = 248 nm) operating at 2 Hz, with a laser fluence of 2 J/cm^2. This film was obtained by using a KTN target containing an excess of 50 % of potassium in order to compensate the K deficiency due to its high volatility [22]. The film was deposited at 700° C under an oxygen pressure of 30 Pa.

X-ray diffraction (XRD) was performed using a 4-circle texture instrument (D8 Discover Brüker AXS) equipped with a parallel beam Cu $K\alpha_1$ radiation in θ-2θ and φ scan modes. The θ-2θ pattern presented on Fig. 1 shows the 100 preferential orientation of the KTN film without any secondary phase. XRD φ-scan performed on the {110} planes comprised of four quite wide peaks ($\Delta\varphi$ = 7.2°) separated by 90° evidenced an in-plane ordering (*i.e.* in-plane preferential orientations).

3. DESIGN RULES AND FABRICATION OF HIGH FREQUENCY METALLIC TEST STRUCTURES

In order to retrieve complex permittivity variations of the KTN material in a broad frequency range, two kinds of test structures have been designed. The first ones consist of CoPlanar Waveguides (CPW) transmissions lines of different lengths for extracting with accuracy the propagation constant γ. To maximize the interactions between the electromagnetic field and the KTN material, a gap of 4 µm was performed between the central strip and the ground strips. By using a conformal mapping technique on a multilayered substrate [23], it results a characteristic impedance of 19Ω for this transmission line. Metallic losses of CPW lines are reduced using large strips for ground and signal lines. A cross-section of the CPW test structure is shown on Fig. 2(a).

The second ones consist of InterDigitated Capacitors (IDC), in a reflection measurements configuration. It permits us to extract the tunability of the KTN material. A space between each finger of 1 µm enables to consider a high static field value of 400 kV/cm for a dc bias value of 40 V. A Scanning Electron Microscopy (SEM) view of an IDC is shown on Fig. 2(b). All of those structures present the advantage of a monolithic integration.

From a technological point of view, a bilayer of electronic resist (EL 13% / PMMA 3%) has been deposited on the substrate by a spin coating process. As all the materials employed are non conductive, a 50Å thick germanium (Ge) metallization was required to permit the evacuation of the charges before exposition on electron beam lithography (LEICA EBPG 5000-Plus). After the removal of the Ge layer, a Ti/Au bilayer (100 nm / 400 nm) was achieved by a conventional lift-off technique after evaporation.

4. MICROWAVE MEASUREMENTS

The characterization of devices under test was done by using a Vectorial Network Analyzer (VNA) Agilent PNA-X N5247A with microprobes (Cascade Microtech) in a 40 MHz – 67 GHz frequency range.

On Fig. 3(a), we plotted the frequency variations of the propagation constant $\gamma=\alpha+j\beta$ of the CPW lines, where α and β describe respectively attenuation (dB/m) and phase (rad/m) constants. This result was obtained from the measurements of two CPW lines of different lengths; in our case we used lengths of 2000 µm and 2900 µm. Further details on this method can be found elsewhere [24]. From the scattering parameters of these transmission lines, it is also possible to retrieve the frequency dependence of the distributed capacitance and conductance parameters of CPW lines [25], as shown on Fig. 3(b).

Concerning the IDC test structure, as it is loaded at the end of a 1 mm CPW transmission line, we have to de-embed this access line to extract its capacitance C and quality factor Q_{factor}. The method proposed by ref. [24] is performed to eliminate parasitic effects due to the CPW access line to the IDC under test. This procedure allows extracting the admittance Y of the IDC which is made by the capacitance C and the conductance G, as presented in the model of Fig. 4(a).

Fig. 5 shows, at the frequency of 30 GHz, the capacitance extraction and the inverse of quality factor (~ $\tan\delta$) for different bias voltages. A tunability of 64% was obtained under a 40 V bias voltage, which corresponds to a 400 kV/cm static field. This value, in comparison with performances of other materials [26-28], appears to be very impressive. Furthermore, the lack of hysteresis effect on the C-V curve indicates that the KTN film is in a paraelectric phase at room temperature.

In a more sophisticated equivalent circuit of an IDC, the capacitance C can be separated, as shown in Fig. 4(b), with a tunable capacitance C_{KTN} due to the KTN contribution added with a parasitic capacitor C_p which is non-tunable, arising from E-fields in air and direct coupling between digits and ground.

On the basis on the measurements, we plotted the log-log variations of loss tangent versus capacitance. It is shown in the inset of Fig. 5. The loss mechanism was analyzed at low dc electric field, namely for values < 100 kV/cm, so the bias voltage was restricted to 10 V. We obtained a quasi-straight line. Its slope gives the power coefficient n of the relation $\tan\delta=(\varepsilon')^n$. We obtained n=1.41 which it is characteristic of the interaction between the microwave field with soft phonons for which $\tan\delta\sim(\varepsilon')^{3/2}$ was predicted [29]. The interaction of a microwave field with soft modes indicates a dielectric dispersion with a Debye-type relaxation [30].

The tunability of 64% extracted from Fig. 5 takes into account, as seen, the variations due to the tunable part of the IDC, but also of a parasitic capacitance C_p mounted in a parallel configuration. In order to estimate the value of C_p, we simulated (under commercial software HFSS by Ansys) the structure shown in the left-inset of Fig. 6. It consists in removing fingers of the IDC. So in practice, we have a CPW line ended by a gap of 9 µm in our case. By this way, with the help of the S_{11} complex parameter, it is possible to extract the frequency variations of this capacitance, as plotted in the right-inset of Fig. 6. For a frequency of 30 GHz, we have a value for C_p of 9 fF. This value is injected in a C(V) modelization procedure proposed by Chase & al. [31]. In this model, the parasitic capacitance value can be used as a fitting parameter. On Fig. 6, a good agreement between measurements and modelization is obtained for a C_p value of 9 fF. Unfortunately, from a device point of view, the tunability of this capacitance is negligible with respect of the IDC which presents fingers with a space of 1 µm. So, to have the tunability of the material (and not the device), we can shift down this C(V) curve of 9 fF. It results a tunability of 75%.

Concerning the complex permittivity extraction of the KTN thin film, although it is possible to calculate it with the knowledge of the propagation constant, we achieved it with values of lineic capacitance and conductance (as shown on Fig. 3(b)) in order to cancel the doubts on the conductivity and thickness of the metal layer.

On Fig. 7(a) we plotted extractions results, up to 67 GHz, of the complex permittivity of the KTN. It was achieved by the measurements CPW transmission lines using the method explained in ref. [32] : it is based on Simplex and Powell optimization algorithms applied on the complex permittivity determination. This retrieval method consists in doing an iterative comparison process between measurements and electromagnetic modelling on the HF2D software [33]. For each iteration, a complex permittivity value, chosen on a two dimensions domain, is affected to the KTN thin film. For this complex value, the HF2D software calculates the conductance G and the capacitance C. Then, they are compared to the measured ones by means of an error function. When this error function reaches a specific criterion, the iterative process stops and gives as a result the complex permittivity value which best minimizes the error function. This procedure was repeated for each frequency point, so it presents the main advantage to be broad-band method. It is to be noted that the two-dimensional area in which the iterative process takes values of complex permittivity under test is established by means of a Latin Hypercube Sampling (LHS) technique and it is highly dependent of the computing power resources. Indeed, a LHS algorithm permits easily the establishment of a list, composed of a couple of points (real and imaginary part of permittivity), which are equi-distributed on a huge two-dimensional area for which the error function is calculated. This one will take a level-surface shaped curve and its wells (often, just a few) will contain the potential solutions. Each well permits to target a smaller two-dimensional

domain, wherein the iterative process can converge (or not) towards a couple that strongly minimizes the error function and which will therefore be solution.

From a physical point of view, the conclusions obtained by the IDC measurements permit to deduce that the permittivity dispersion can be treated by a quasi-Debye model, and this assessment is stressed also by the plotting of the CPW line complex characteristic impedance evolution, shown on Fig. 8. Due to the fact that the gap between central conductor and lateral ground metallic conductors are only of 4µm, the line is highly mismatched with respect of the 50Ω presented by the microprobes. The real part of the characteristic impedance is dominated by the resistive part of the line in low frequencies, which explain the hyperbolic shaped curve obtained.

Concerning the imaginary part, it is directly proportional to the term [($GL\omega$)-($RC\omega$)], with ω the angular frequency and R, L, C and G respectively the lineic values of resistance, inductance, capacitance and conductance of the CPW line. Obviously, the imaginary part of Z_c exists if the structure exhibits losses. In our case, below 30 GHz, this part appears to be negative, and becomes positive above. This positive sign is given by a product value of GL higher than the RC one. As the frequency variations of the inductance are tenuous, it is shown here that the values taken by G are huge with growing frequency. Furthermore, this trend is reinforced by the decrease of C values, as shown in Fig. 3(a). As G is related to ε" and C to ε' ones, the relaxation phenomenon is again put in stress.

In our case, for the fitting by means of a quasi-Debye model, we used a Cole-Davidson model (which presents an excess of loss in high frequencies):

$$\varepsilon^*(\omega) = \varepsilon'_\infty + \frac{\varepsilon_s^* - \varepsilon'_\infty}{(1 + j\omega\tau)^\beta} \quad (1)$$

where ε'_∞ and ε_s^* are respectively the high and low frequency permittivity values and τ is the distribution centre of relaxation time. The β exponent, which makes a deviation of the pure Debye model when different of 1, indicates the variance of this distribution.

Parameters of the Cole-Davidson model were determined by fitting the complex dielectric dispersion, and permit to retrieve a relaxation time τ=2.8ps and a power coefficient β=0.6 was estimated. ε_s^* can be easily extracted as ε_s^*=355-10j on the basis of low frequency measurements performed on IDC and conformal mapping technique.

On Fig. 7(b), we plotted the loss tangent tanδ, which corresponds to the ratio between the imaginary part and the real part of the permittivity. It presents a huge increase of its value with growing frequency, and reaches 60% at 67 GHz. This high value is, for the moment, prohibitive for practical applications at so high frequency. However, up to X and

K_u band (12 GHz and 18 GHz respectively), this material appears to be a serious candidate for tunable applications with regards of its huge tunability and loss tangent value.

5. CONCLUSION

A 400 nm thick $KTa_{0.65}Nb_{0.35}O_3$ layer deposited on MgO substrate was characterized up to 67 GHz by means of coplanar transmission lines and interdigitated capacitors. By means of an application of dc electric field, the capacitance exhibits a tunability of 64% for E_{dc}=400 kV/cm at 30 GHz and room temperature and the complete device. We showed that parasitic elements on a CID configuration minimize this value, which reached 75% by means of an accurate study. The specific composition 65/35, in paraelectric phase, whose Curie temperature is expected to be close to room temperature explains this huge value. It is comparable with the one obtained on a 50/50 composition (in a ferroelectric phase at room temperature) for E_{dc}=70 kV/cm on a stub at 10 GHz [21]. Then, a frequency dispersion study of the complex permittivity was performed. A dielectric relaxation is observed and can be modelized by a Cole-Davidson model. However, the frequency variations of the loss tangent exhibit high values with increasing frequency: close to 10% at 10 GHz and reaches 60% at 67 GHz. An optimization of the deposition process, by means of heterostructures or by doping, is of a prime importance to target a compromise between high tunability and low loss suitable for high frequency applications such as tunable filters for instance.

ACKNOWLEDGMENT

The authors would like to thank K. Blary, from IEMN (university of Lille 1), for the fabrication of the devices.

REFERENCES

[1] J. F. Scott, F.M. Ross, C. A. De Araujo Paz, M. C. Scott, and M. Huffman, "Structure and device characteristics of SrBi2Ta2O9-based nonvolatile random-access memories," *MRS Bulletin*, vol. 21, pp. 33–39, Jul. 1996.

[2] N. Setter, D. Damjanovic, L. Eng, G. Fox, S. Gevorgian, S. Hong, A. Kingon, H. Kohlstedt, N. Y. Park, G. B. Stephenson, I. Stolitchnov, A. K. Tagantsev, D. V. Taylor, T. Yamada, and S. Streiffer, "Ferroelectric thin films : review of materials, properties and applications," *Jour. of Appl. Phys.*, vol. 100, art. no. 051606, 2006.

[3] H. Robinson, C. W. Pitt, and R. A. Gibson, "Silicon lithium niobate electro-optic waveguide modulator structures in the parallel-plate configuration," *Appl. Opt.*, vol. 32, pp. 3981–3988, 1993.

[4] M. J. Lancaster, J. Powell, and A. Porch, "Thin-film ferroelectric microwave devices," *Supercond. Sci. Technol.*, vol. 11, pp. 1323–1334, 1998.

[5] G. Velu, L. Burgnies, G. Houzet, K. Blary, D. Lippens, and J. C. Carru, "Characterization of ferroelectric films up to 60 GHz : application to phase shifters," *Integr. Ferroelectr.*, vol. 93, pp. 110–118, 2007.

[6] I. V. Shadrivov, S. K. Morrison, and Y. S. Kivshar, "Tunable split-ring resonators for nonlinear negative-index metamaterials," *Opt. Expr.*, vol. 14, pp. 9344–9349, 2006.

[7] F. Zhang, L. Kang, Q. Zhao, J. Zhou, X. Zhao, and D. Lippens, "Magnetically tunable left handed metamaterials by liquid crystal orientation," *Opt. Expr.*, vol. 17, pp. 4360–4366, 2009.

[8] T. R. Tsai, C. Y. Chen, C. L. Pan, R. P. Pan, and X. C. Zhang, "Terahertz time-domain spectroscopy studies of optical constant of the nematic liquid crystal 5CB," *Appl. Opt.*, vol. 42, pp. 2372–2376, 2003.

[9] L. C. Sengupta, and S. Sengupta, "Breakthrough advances in low loss, tunable dielectric materials," *Mater. Res. Innov.*, vol. 2, pp. 278–282, 1999.

[10] M. Ouaddari, S. Delprat, F. Vidal, M. Chaker, and K. Wu, "Microwave characterization of ferroelectric thin-film materials," *IEEE Trans. Microw. Theory Tech.*, vol. 53, no. 4, pp. 1390–1397, Apr. 2005.

[11] B. Ouagague, H. B. El-Shaarawy, S. Pacchini, S. Payan, A. Rousseau, M. Maglione, and R. Plana, "BST tunability study at DC and microwave frequencies by using IDC and MIM capacitors," *Asia-Pacific Microw. Conf.*, Yokohama, Japan, pp. 1837–1840, Dec. 2010.

[12] S. S. Gevorgian, "Ferroelectrics in microwave devices circuits and systems," 1st ED., London: Springer-Verlag, 2009.

[13] J. Venkatesh, V. Sherman, and N. Setter, "Synthesis and dielectric characterization of potassium niobate tantalite ceramics," *J. Am. Ceram. Soc.*, vol. 88, no. 12, pp. 3397–3404, 2005.

[14] A. C. Carter, J. S. Horwitz, D. B. Chrisey, J. M. Pond, S. W. Kirchoefer, and W. Chang, "Pulsed laser deposition of ferroelectric thin films for room temperature active microwave electronics," *Integr. Ferroelectr.*, vol. 17, pp. 273–285, 1997.

[15] V. Laur, A. Rousseau, G. Tanné, P. Laurent, S. Députier, M. Guilloux-Viry, and F. Huret, "$KTa_{0.6}Nb_{0.4}O_3$ ferroelectric thin film behavior at microwave frequencies for tunable applications," *IEEE Trans. Ultrason. Ferroelectr., Freq. Control*, vol. 53, no.12, pp. 2280–2286, Dec. 2006.

[16] S. Triebwasser, "Study of ferroelectric transitions of solid-solution single crystals of $KNbO_3$-$KTaO_3$," *Phys. Rev.*, vol. 114, pp. 63–70, 1959.

[17] D. Rytz, and H. J. Scheel, "Crystal growth of $KTa_{1-x}Nb_xO_3$ solid solutions by a slow-cooling method," *J. Cryst. Growth*, vol. 59, no. 3, pp. 468–484, Oct. 1982.

[18] S. E. Moon, E. K. Kim, M. H. Kwak, H. C. Ryu, Y. T. Kim, K. Y. Kang, and S. J. Lee, "Orientation dependent microwave dielectric properties of ferroelectric $Ba_{1-x}Sr_xTiO_3$ thin films," *Appl. Phys. Lett.*, vol. 83, art. no. 2166, 2003.

[19] T. Delage, C. Champeaux, A. Catherinot, J. F. Seaux, V. Madrangeas, and D. Cros, "High-K BST films deposited on MgO by PLD with and without buffer-layer," *Thin Solid Films*, vol. 453-454, pp. 279–284, Apr. 2004.

[20] L. Zhang, V. Laur, A. Pothier, Q. Simon, P. Laurent, N. Martin, M. Guilloux-Viry, and G. Tanné, "KTN ferroelectrics-based microwave tunable phase shifter," *Microw. Opt. Tech. Lett.*, vol. 52, no. 5, pp. 1148–1150, 2010.

[21] Q. Simon, Y. Corredores, X. Castel, R. Benzerga, R. Sauleau, K. Mahdjoubi, A. Le Febvrier, S. Députier, M. Guilloux-Viry, L. Zhang, P. Laurent, and G. Tanné, "Highly tunable microwave stub resonator on ferroelectric $KTa_{0.5}Nb_{0.5}O_3$ thin film," *Appl. Phys. Lett.*, vol. 99, art. no. 092904, 2011.

[22] A. Rousseau, V. Laur, M. Guilloux-Viry, G. Tanné, F. Huret, S. Députier, A. Perrin, F. Lalu, and P. Laurent, "Pulsed laser deposited $KNbO_3$ thin films for applications in high frequency range," *Thin Solid Films*, vol. 515, no. 4, pp. 2353–2360, Dec. 2006.

[23] S. S. Gevorgian, P. L. J. Linner, and E. Kollberg, "CAD models for shielded multilayered CPW," *IEEE Trans. Microw. Theory Tech.*, vol. 43, no. 4, pp. 772–779, Apr. 1995.

[24] L. Burgnies, G. Velu, G. Houzet, K. Blary, J. C. Carru, and D. Lippens, "A TRL-like calibration for tunable interdigitated BST varactors," *IEEE Trans. Instr. Meas.*, vol. 57, no. 6, pp. 1127–1132, June 2008.

[25] D. F. Williams, U. Arz, and H. Grabinski, "Characteristic-impedance measurement error on lossy substrates," *IEEE Microw. Wireless Compon. Lett.*, vol. 11, no. 7, pp. 299–301, July 2001.

[26] L. Yang, F. Ponchel, G. Wang, D. Remiens, J. F. Legier, D. Chateigner, and X. Dong, "Microwave properties of epitaxial (111)-oriented $Ba_{0.6}Sr_{0.4}TiO_3$ thin films on Al_2O_3(0001) up to 40 GHz," *Appl. Phys. Lett.*, vol. 97, art. no. 162909, 2010.

[27] G. Houzet, L. Burgnies, G. Velu, J. C. Carru, and D. Lippens, "Dispersion and loss of ferroelectric $Ba_{0.5}Sr_{0.5}TiO_3$ thin film up to 110 GHz," *Appl. Phys. Lett.*, vol. 93, art. no. 053507, 2008.

[28] E. Defäy, T. Lacrevaz, T. T. Vo, V. Sbrugnera, C. Bermond, M. Aïd, and B. Flechet, "Ferroelectric properties of $Pb(Zr,Ti)O_3$ thin films until 40 GHz," *Appl. Phys. Lett.*, vol. 94, art. no. 052901, 2009.

[29] A. K. Tagantsev, V. O. Sherman, K. F. Astafiev, J. Venkatesh, and N. Setter, "Ferroelectric materials for microwave tunable applications," *Jour. Electroceram*, vol. 11, pp. 5–66, 2003.

[30] G. Artl, U. Bottger, and S. Witte, "Emission of GHz shear waves by ferroelastic domain walls in ferroelectrics," *Appl. Phys. Lett.*, vol. 63, pp. 602–604, 1993.

[31] D. R. Chase, L. Y. Chen, and R. A. York, "Modeling the capacitive nonlinearity in thin-film BST varactors," *IEEE Trans. Microw. Theory Tech.*, vol. 55, no. 10, pp. 3215–3220, Oct. 2005.

[32] T. Lacrevaz, B. Flechet, A. Farcy, J. Torres, M. Gros-Jean, C. Bermond, T. T. Vo, B. Blampey, G. Angenieux, J. Piquet, and F. de Crecy, "Wide band frequency and in situ characterisation of high permittivity insulators (High-K) for H.F. integrated passives," *Microelec. Eng.*, vol. 83, pp. 2184–2188, 2006.

[33] F. Charlet, C. Bermond, S. Putot, G. Le Carval, and B. Flechet, "Extraction of (R,L,C,G) interconnect parameters in 2D transmission lines using fast and efficient numerical tools," *Int. Conf. on Simulation of Semiconductor Processes and Devices*, SISPAD2000, Seattle, USA, pp. 87–89, Sept. 2000.

FIGURE CAPTIONS

FIG. 1. θ-2θ X-ray diffraction pattern of the $KTa_{0.65}Nb_{0.35}O_3$ film grown on (100)MgO.

FIG. 2. (a) Cross-section of a CPW line and (b) SEM view of an IDC pattern.

FIG. 3. (a) Complex propagation constant variations and (b) CPW line capacitance and conductance parameters variations from 40 MHz to 67 GHz.

FIG. 4. (a) Equivalent circuit and (b) identification of the different capacitive contributions of an IDC.

FIG. 5. C-V characteristics and inverse quality factor of IDC measured at 30 GHz and at room temperature. The inset shows the log-log representation of loss tangent vs capacitance.

FIG. 6. Measurements (square symbols) vs. modelization (circle symbols) of the capacitance-voltage characteristics at 30GHz. At the top-right hand corner, the frequency evolution of the parasitic capacitance of the CID, used as a fitting parameter in the modelization and obtained under the HFSS software. At the top left-hand corner, the structure simulated.

FIG. 7. (a) Measurements (symbols) and simulation (lines) of the KTN thin film complex permittivity evolution and (b) of its loss tangent.

FIG. 8. Complex characteristic impedance of CPW line from 40 MHz to 67 GHz.

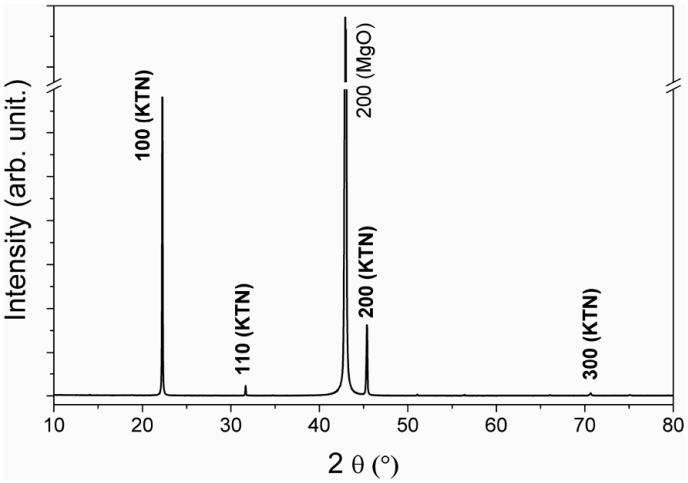
Intensity (arb. unit.)
100 (KTN)
110 (KTN)
200 (MgO)
200 (KTN)
300 (KTN)
10
20
30
40
50
60
70
80
2 θ (°)

Fig. 1

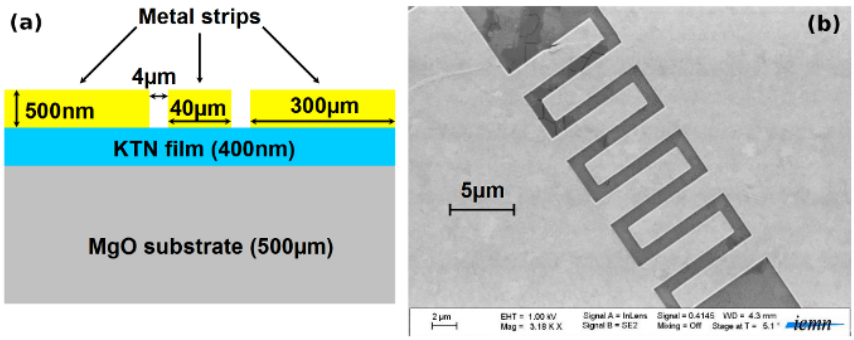
(a)
Metal strips
4μm
500nm
40μm
300μm
KTN film (400nm)
MgO substrate (500μm)
(b)
5μm

Fig. 2

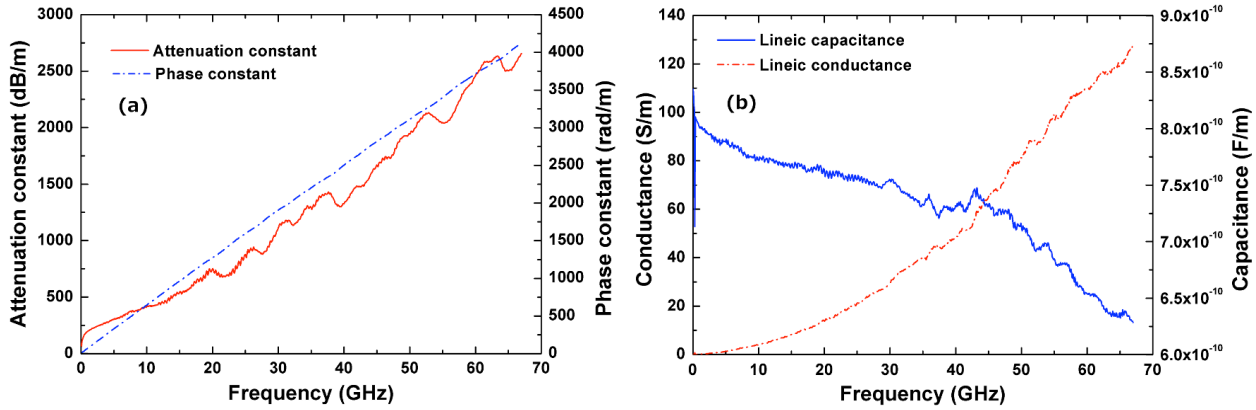
Attenuation constant
Phase constant
(a)
Attenuation constant (dB/m)
Phase constant (rad/m)
Frequency (GHz)
Lineic capacitance
Lineic conductance
(b)
Conductance (S/m)
Capacitance (F/m)
Frequency (GHz)

Fig. 3

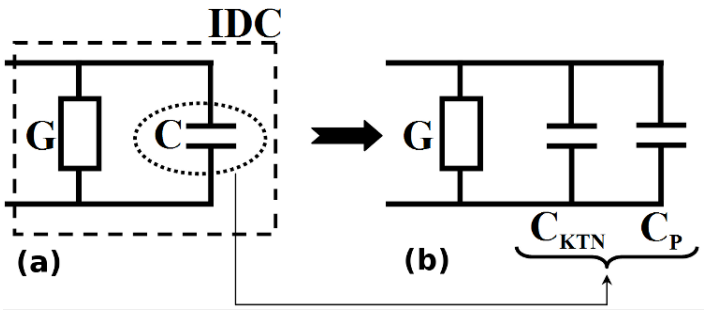

Fig. 4

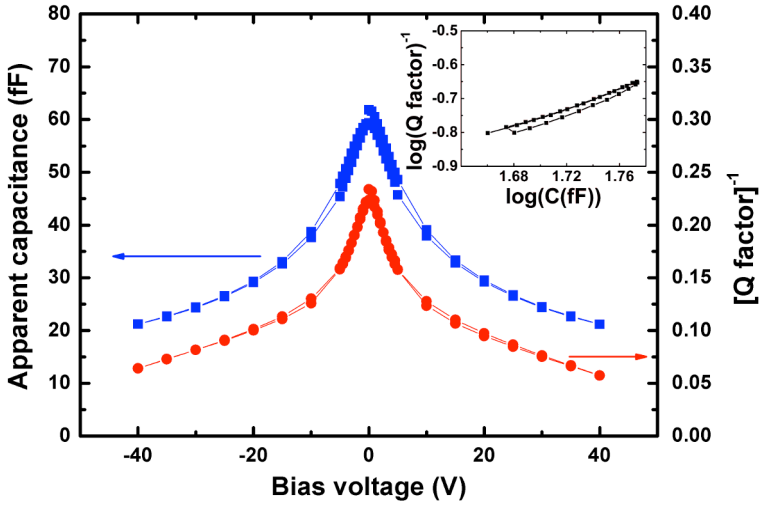
Apparent capacitance (fF)
[Q factor]$^{-1}$
Bias voltage (V)
log(Q factor)$^{-1}$
log(C(fF))
80
70
60
50
40
30
20
10
0
0.40
0.35
0.30
0.25
0.20
0.15
0.10
0.05
0.00
-40
-20
0
20
40
-0.5
-0.6
-0.7
-0.8
-0.9
1.68
1.72
1.76

Fig. 5

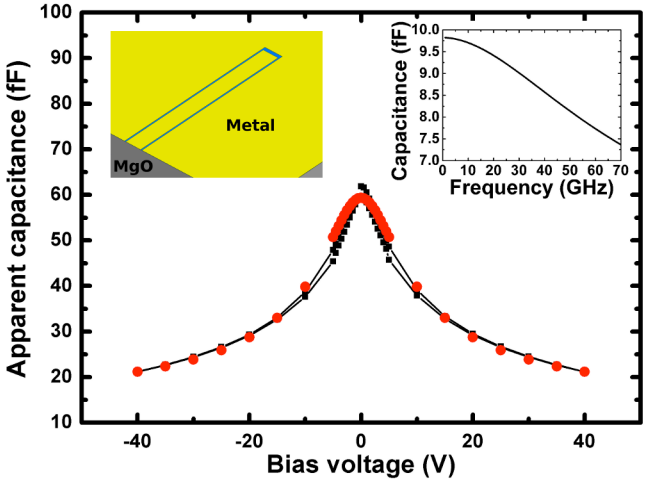
Apparent capacitance (fF)
Bias voltage (V)
Metal
MgO
Capacitance (fF)
Frequency (GHz)

Fig. 6

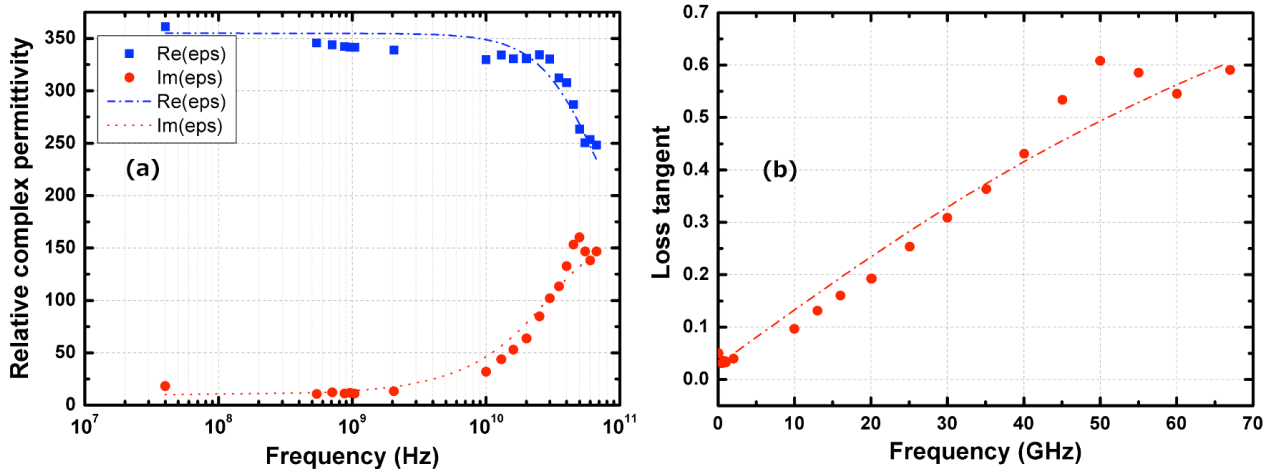
Relative complex permittivity
Re(eps)
Im(eps)
Re(eps)
Im(eps)
(a)
Frequency (Hz)
Loss tangent
(b)
Frequency (GHz)

Fig. 7

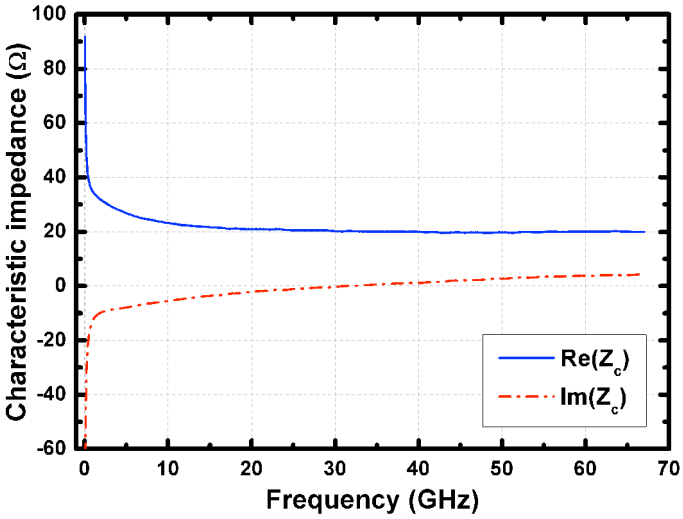
Characteristic impedance (Ω)
Frequency (GHz)
Re(Z_c)
Im(Z_c)
100
80
60
40
20
0
-20
-40
-60
0
10
20
30
40
50
60
70

Fig. 8